



# Study of corrosion properties of carbon steel, 304 and 316L stainless steels in sulfuric acid and their degradation products

Eakapoj KHAMME<sup>1,\*</sup>, and Rachsak SAKDANUPHAB<sup>1</sup>

<sup>1</sup> Department of Manufacturing System Technology, College of Advanced Manufacturing Innovation, King Mongkut's Institute of Technology Ladkrabang, Bangkok 10520, Thailand

\*Corresponding author e-mail: akekapoj@gmail.com

## Received date:

10 March 2023

## Revised date

6 September 2023

## Accepted date:

9 September 2023

## Keywords:

Sulfuric acid;  
Corrosion properties;  
Carbon steel;  
SS304;  
SS316L

## Abstract

In this study, corrosion properties of carbon steel and stainless steels, and degradation of sulfuric acid by the corrosion mechanism are presented. Carbon steel (CS), 304 stainless steel (SS304), and 316L stainless steel (SS316L) specimens were analyzed through their electrochemical response by using a potentiostat measurement. The specimens were submerged in concentrated 98 wt.% of H<sub>2</sub>SO<sub>4</sub> acid for 0 day to 60 day. The degradation of H<sub>2</sub>SO<sub>4</sub> was determined by its volume change, turbidity, and color due to the corrosion mechanism. Corrosion rate of CS, SS304 and SS316L specimens are 43.237 mm/year, 0.420 mm/year and 0.086 mm/year, respectively. After 60 days, the weight-loss of CS, SS304 and SS316L specimens are 48 wt%, 33 wt% and 0.1 wt%, respectively. Corrosion resistance of the materials are influenced by the passive oxide layer that forms on its surface and associated with electrochemical activity or semiconductive composition. The degradation of H<sub>2</sub>SO<sub>4</sub> acid was observed due to the corrosion process of specimens and related to the turbidity and volume increase while the wt% concentration of H<sub>2</sub>SO<sub>4</sub> acid decreases. In order to make material choices that enable continuous and safe operation of the process, it is important to understand the corrosion mechanism changes.

## 1. Introduction

Carbon steel and stainless steels materials are commonly used in the process industry, including reactors, valves, pipes, mixers, and storage tanks. Process equipment is usually made from stainless steel, but the alloying depends on the corrosiveness of the environment. The selection of a proper stainless-steel grade is crucial for the designed lifetime of the equipment. Austenitic stainless-steel types SS304 and SS316L are the well-known alloys for the H<sub>2</sub>SO<sub>4</sub> storage tanks while CS is also commonly used due to the relatively cheap initial cost. When the CS contact with H<sub>2</sub>SO<sub>4</sub> acid, the hydrogen gas and ferrous ions react on the surface of CS and formation of ferrous sulfate (FeSO<sub>4</sub>) protective layer [1]. To determine whether the selected suitable stainless steel grade for a specific industrial application is conducted based on the characteristics of the environment, but often limited by the foreseen lifecycle costs. It is influenced by the concentration of the solution, moisture content, exposure or operating temperature, oxygen content, water content, flow rate, passive film on the stainless steel surface, and others. The stability of passive films and the elemental makeup of stainless steel surfaces have an impact on how well they resist corrosion [2]. The stability of passive film is influenced by the chemistry of an alloy and the pH of the surrounding environment. When the pH is reduced, the chromium oxide film becomes more stable, and when the pH is increased, the iron oxide layer becomes more stable. [3]. Other than the formation on second phase (e.g., sulfide) of passive film could induce heterogeneities and defects

(chromium depletion) due to the corrosion attack under high pH [4]. The enriched chromium diffusion is due to the fine microstructure and homogeneous growth of the passive film [5]. The more consistent and durable passive film that is created on stainless steel affects the enhancement of the metal's electrochemical properties in hostile environments. Which is the limitation of stainless steel in concentrated acid conditions. Numerous journals have published studies on the corrosive properties of sulfuric acid on metal surfaces in terms of corrosion rate and concentration [6]. On the other hand, the volume change and turbidity of sulfuric acid after corrosion have received very few observations. This volume change of corrosion has an effect on the sulfuric acid concentration and a change in color or turbidity. These will complement previous research. As well as being able to explain the changes actually occurred in large-scale industrial processes in an open system. This situation is not seen in closed storage or in industrial procedures where sulfuric acid is rotated for a short period.

## 2. Experimental

### 2.1 Materials

Specimens used in this study were commercial grade metal plate of CS, SS304 and SS316L with dimension of 30 mm × 100 mm × 5 mm. The specimens were grinded with silicon carbide papers of 180 grit to 1200 grit size under running water. After that they were cleaned with acetone, deionized (DI) water and dried in the oven at the temperature

105 ± 5°C for 4 h. The specimens were kept in a desiccator before doing the experiments. H<sub>2</sub>SO<sub>4</sub> solution (98 wt%) from LG International (S'Pore) PTE., LTD was used in the experiment.

## 2.2 Methods

Corrosion properties of the CS, SS304 and SS316L specimens in H<sub>2</sub>SO<sub>4</sub> solution were analyzed through their electrochemical response by using an AUTOLAB PGSTAT302N potentiostat with a compliance voltage of 30 V and a bandwidth of 1 MHz, combined with FRA32M module with frequency response analyzer NOVA software. The three electrodes cell configuration was employed to investigate the electrochemical behavior of the specimens. The polished specimens with exposed surface area of 10 mm<sup>2</sup> served as a working electrode in this cell. The saturated calomel electrode, (0.242 V SHE (Standard Hydrogen Electrode) and platinum coil were used as reference and counter electrodes, respectively. The electrochemical testing was carried out in H<sub>2</sub>SO<sub>4</sub> at pH 1. The pH of the electrolyte was measured within the tolerance of ± 0.1 by the 827 pH Lab Meter. The specimens were immersed in electrolyte immediately after preparation. The potential of each specimen was obtained after open circuit potential (OCP) stabilization. To investigate the corrosion behavior and barrier properties of the passive film, the polarization test was executed at a rate of 300 mV.s<sup>-1</sup> from -1.0 V to 1.5 V vs OCP. All the electrochemical testing was performed at ambient temperature.

The corrosion rate of specimens was analyzed by weight-loss from experiment comparing the weight difference of metal plate specimens soaked in H<sub>2</sub>SO<sub>4</sub> at 98 wt% concentration for 0 day to 60 days at the laboratory test conditions. The weight-loss was used for analysis corrosion rates in unit of mass per year. For the weight-loss test, the metal plate tested were immersed in H<sub>2</sub>SO<sub>4</sub> at 98 wt% concentration. Three different material specimens of the test contained separately in 150 mL glass bottle for 60 days at laboratory temperatures under open system. At the end of test, cleaned by DI water, acetone rinsed, dried, and reweighed. The corrosion rates were analyzed by Equation (1):

$$\text{Corrosion Rate (mm/year)} = W_{\text{loss}}/\rho \times a \times t \quad (1)$$

where  $W_{\text{loss}}$  is the weight-loss (g),  $\rho$  is the density (g.cm<sup>-3</sup>),  $a$  is the area (cm<sup>2</sup>) and  $t$  is the time of exposure (year).

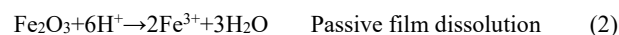
The degradation of H<sub>2</sub>SO<sub>4</sub> products was determined by its volume change, turbidity, and color due to corrosion mechanism. The turbidity of acid solution was analyzed using turbidity meter (Eutech TN-100) applying the ISO 7027 measurement method, compliance nephelometric non-ratio method (90°) using Infrared-emitting diode system ( $\lambda = 850$  nm) as the light source. The acid solution density and concentration were measured by Mettler Toledo DM45 and Metrohm 888 Titrand, respectively. Weight-loss test, scanning electron microscopy (SEM) and energy dispersive X-ray spectroscopy (EDS) (OXFORD x-max 20) were used for the corrosion, surface morphology and elemental compositions analysis, respectively.

## 3. Results and discussion

### 3.1 Corrosion properties of CS, SS304 and SS316L in H<sub>2</sub>SO<sub>4</sub> solution

#### 3.1.1 Polarization curves ( $I_{\text{corr}}$ , $E_{\text{corr}}$ and Corrosion rate)

The peak potential of the CS in the H<sub>2</sub>SO<sub>4</sub> polarization curves is an alternating active-passive phenomenon that frequently takes place, as seen in Figure 1. The form of hydrated ferric ions of metal iron in the passive state was dissolved since the hydrated ferrous ions of metal iron in the active state were also dissolved in the solution, proving that the passive film is ferric oxide (Fe<sub>2</sub>O<sub>3</sub>). It is possible to visualize these reactions as happening simultaneously using Equation (2).

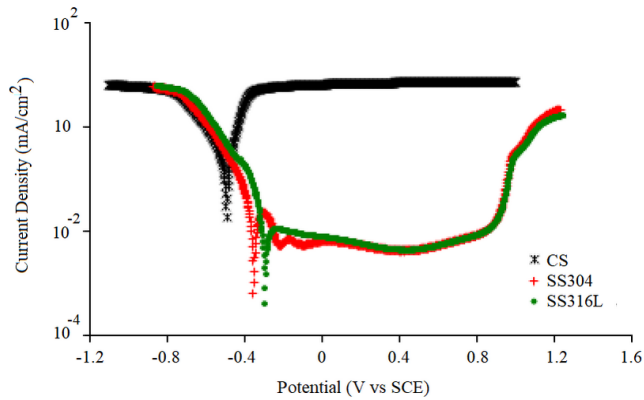


The periodic conversion of active and passive causes the vibration of potential and predicts competition would impact and degrade the passive film [7]. The hydrogen evolution reaction inhibits both the cathode and anode reactions. The diffusion mass transfer of ferrous ions or ferrous sulfate regulates the corrosion of CS in H<sub>2</sub>SO<sub>4</sub>. According to Figure 1, which also shows the polarization curves of SS304, the potential increased from -0.356 V (vs SCE) to 0.831 V (vs SCE). As Cr-rich oxide nuclei were produced in oxide films during the initial stage of oxidization, the rate of corrosion dramatically decreased. It is hypothesized that the oxide formed when Fe and Ni were selectively dissolved by solid-state processes, and that it then expanded because of the precipitation of extraneous metallic ions. This is the asymmetrically structured hematite, whose formula is  $\alpha\text{-(Fe,Cr)}_2\text{O}_3$  and which has a non-stoichiometric composition. Because the larger oxide nuclei on the surface are pressed away by the smaller inner particles created at the subsurface layer, increasing immersion time has the effect of starting a finer and more ordered outer surface layer [8]. When the potential is higher than 0.831 V (vs SCE), the current density increases considerably. This is allegedly related to the pitting corrosion.

The polarization curve for the SS316L specimen exhibits conventional passive self-balancing but does not show an active-passive area. The passive zone of SS316L was from -0.292 V (vs SCE) to 0.829 V (vs SCE), as shown in Figure 1. When Cr is enriched, an oxide coating forms on the metal's surface, preventing the solubility of Fe<sup>2+</sup> ions in the active region. Owing to the chromium's neat time oxidation to Cr<sup>3+</sup> ions and hydrolysis process, which creates a hydrated oxide film (Cr(OH)<sub>3</sub>) [9]. The faulty oxide film was created by the rising current that occurred during anode polarization. The considerable stability of Fe<sup>2+</sup> species was shown by the current density, which increased significantly beyond 0.829 V (vs SCE). The  $E_{\text{corr}}$  value has changed from negative to positive, which is typical and thought to be a result of the thickness of the passive film. On the other hand, after anode polarization, tiny holes on the specimen surface are responsible for the decrease in  $E_{\text{corr}}$ . Table 1 provides a summary of the electrochemical corrosion kinetics characteristics, i.e., corrosion potential ( $E_{\text{corr}}$ ), corrosion current density ( $I_{\text{corr}}$ ) and corrosion rate (obtained from extrapolating the polarization curves).

**Table 1.** Quantitative information obtained from the cyclic polarization curves.

Materials	$E_{\text{corr}}$ (V)	$I_{\text{corr}}$ (A)	Corrosion rate (mm/year)
CS	-0.4942	3.72E-03	43.237
SS304	-0.3482	3.61E-05	0.420
SS316L	-0.2936	7.42E-06	0.086



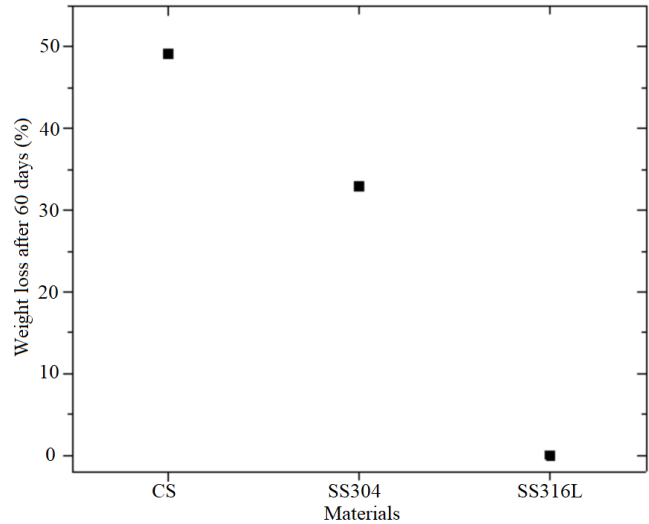
**Figure 1.** Polarization curve of CS, SS304 and SS316L specimens in  $H_2SO_4$  solution.

Table 1 shows the quantitative data of the corrosion parameters of CS, SS304, and SS316L specimens in  $H_2SO_4$  solution. For CS, SS304, and SS316L readings of, respectively,  $-0.4942$  V,  $-0.3482$  V, and  $-0.2936$  V vs. SCE, further negative  $E_{corr}$  values were discovered.  $I_{corr}$  was measured simultaneously using CS, SS304, and SS316L at  $3.72 \times 10^{-3}$ ,  $3.61 \times 10^{-5}$ , and  $7.42 \times 10^{-6}$  A, respectively. The values for  $E_{corr}$  and  $I_{corr}$  show how stable a passive film is. Because the SS316L specimen's finer polygonal oxide film structure had a more stable and limited number of MnS inclusions, its  $E_{corr}$  was lower than that of the SS304 specimens [10]. When SS316L has both a strong corrosion resistance and low corrosion rate. This is a result of the synergic effect of Mo, Fe, Cr and S. Because of the synergic effect of Mo, Fe, Cr and S in SS316L, the synergic effect of Cr and Fe was less effective than the effect of adding 16 wt% Cr in SS304 [11]. The passive layer stability of stainless steels decreases in the presence of less than 1% of Mo by weight of material and increases sequentially when Mo >1% to 3% by weight [12].

### 3.1.2 Weight-loss of specimens in $H_2SO_4$ solution

Figure 2 shows the calculated corrosion rate value obtained from weight-loss measurement. When compared to SS316L, CS and SS304 exhibit more aggressive corrosion. As a result, for applications involving acid storage, SS316L has a longer service life and is generally safer than CS and SS304.

The composition of the passive film is additionally impacted by the corrosion conditions on the surface of metal objects. The SS316L specimen's corrosion resistance in  $H_2SO_4$  was the best, whereas the CS specimen was the lowest. They are associated with electrochemical activity or semiconductive composition.  $Fe_2O_3$  and  $Fe_2SO_4$  made up the surface film on the CS when it was submerged in the  $H_2SO_4$ ;  $Fe_2O_3$ ,  $Fe_2SO_4$ , and  $Cr_2O_3$  made up the surface film on the SS304; and  $Fe_2O_3$ ,  $Cr_2O_3$ ,  $MoO_3$ , and  $Fe_2SO_4$  made up the surface film on the SS316L. In addition, it was reported in several sources that the applied potential had a variety of effects on the composition and protective properties of passive films [13]. At the open circuit potential (OCP),  $Cr_2O_3$ ,  $Cr(OH)_3$ , and Fe form passive films, whereas at the  $-100$  mV SCE, FeO,  $Fe_2O_3$ , FeOOH, and  $Cr_2O_3$  exhibit nearly identical compositions. However, the passive film generated at OCP is 1.11 contrast,  $-100$  mV SCE is 0.31, and the major element fraction was changed by the element ratio of Cr/Fe [14].



**Figure 2.** The weight-loss of CS, SS304 and SS316L specimens after 60 days for immersion in  $H_2SO_4$ .

### 3.1.3 Surface morphology of specimens

Figure 3 shows the SEM images of specimen surfaces before and after immersed in the  $H_2SO_4$  for 60 days. All specimens present rough surface with minimal scratches due to sandpaper polishing. Pit holes, fissures, and uneven surfaces can be seen more clearly at 500X and 1.00KX. After being immersed in the  $H_2SO_4$  for 60 days,

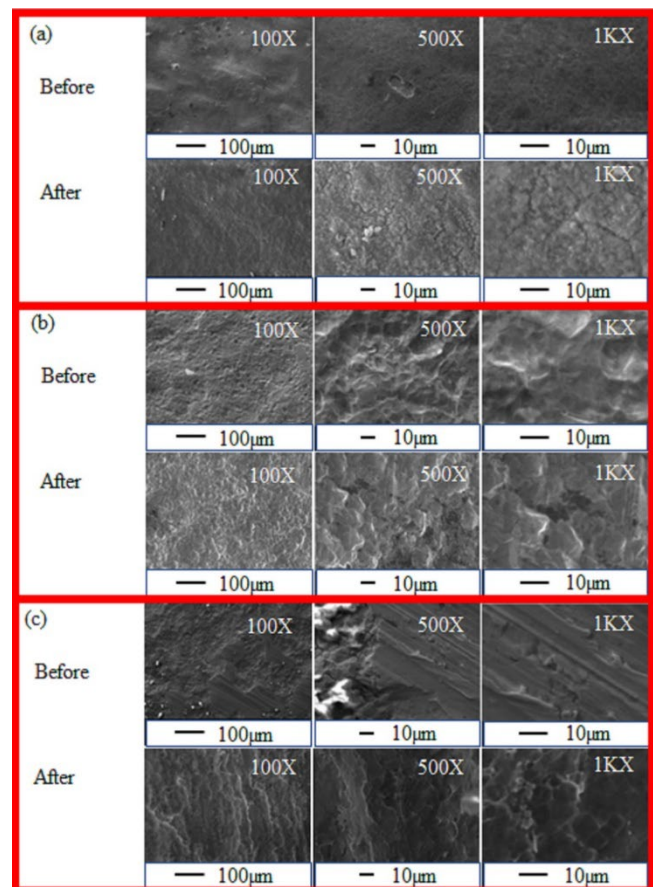


**Figure 3.** SEM images at 100X, 500X and 1.00KX of CS (a), SS304 (b), and SS316L (c) specimens before and after immersion in  $H_2SO_4$  for 60 days.

the surface was extensively corroded and the rust spots were evenly distributed, as shown in Figure 3(b) at a 100X magnification. There were white flecks and little black holes. The silica-based particles were distributed haphazardly across the amorphous surface, a trait that has also been seen in other studies [15]. With a 500X magnification, the rough surface with its dark holes and crevices could be clearly observed. At a magnification of 1.00KX, similar surface morphology and more distinct images of the distributed rust spots were discernible. The samples have experienced severe corrosion, which has caused blisters to form and eventually burst.

Figure 3(b), which is 100X magnified, demonstrates the surface corrosion that has taken place as well as the development of the passive layer. At a 500X magnification, the SEM picture showed that some locations had surface passive film coatings while other parts had corroded due to corrosive deterioration. There is a general form of corrosion. Although the degree of damage is less severe, it is like the micrographs acquired from CS (Figure 3(a)). When viewed at 1.00KX magnification, the surface of the SS304 specimen was coated in white precipitation, some of which had scattered black holes at several stigmas. This indicates that the test media caused the SS304 specimens to fail due to significant general corrosion. The selective dissolving abilities of the Cr alloy and the buildup of  $\text{Cr}_2\text{O}_3$  are said to affect the surface structure of the passive film layer, according to several investigations. Moreover, because of the greater quantities of species  $\text{SO}_4^{2-}$ , it was pierced by sulfate ions, leading to pore corrosion and a decrease in passive film repair [16].

The surface of the SS316L that was partially covered with a black film (passive film) and its rough surface are illustrated in Figure 3(c) at a magnification of 100X. The surface that the passive film completely covered and then flaked off from that area is visible at a magnification of 500X, exposing the surface underlining. As the magnification was increased to 1.00KX, a passive film of corrosion had formed on the metal surface. The acid on the surface had a slight corrosive effect. The corrosion was in a general and pitting type. When compared to SS304, the damage was much less severe (Figure 3(b)). Passive film has collected on the surface of SS316L during the dissolving of  $\text{H}_2\text{SO}_4$ , which is present as sulfur in the nano-passive film. It is widely accepted that the bilayer structure of passive film is enhanced by Cr in the inner layer and Fe in the outer layer [17]. The sulphate ions ( $\text{SO}_4^{2-}$ ) from the  $\text{H}_2\text{SO}_4$  are the primary species involved in the corrosion reaction. By penetrating through the passive layer, these ions shatter the protective chromium film on the stainless-steel surface (film rupture), which starts active interfacial corrosion reactions at the specimen surface [18].

## 3.2 Degradation of $\text{H}_2\text{SO}_4$ products

### 3.2.1 Turbidity of $\text{H}_2\text{SO}_4$ solution

Figure 4 depicts the change in turbidity of the  $\text{H}_2\text{SO}_4$  solution after immersion in CS, SS304, and SS316L. With the CS specimen, the turbidity of the solution grew to 30 NTU after 3 days and to 80 NTU after 30 days of immersion. The turbidity of the solution in which SS304 was immersed, however, was steady for 7 days before rising to 20 NTU after 15 days of immersion. Two linear slopes were thought to form as the turbidity changed: the first slope runs

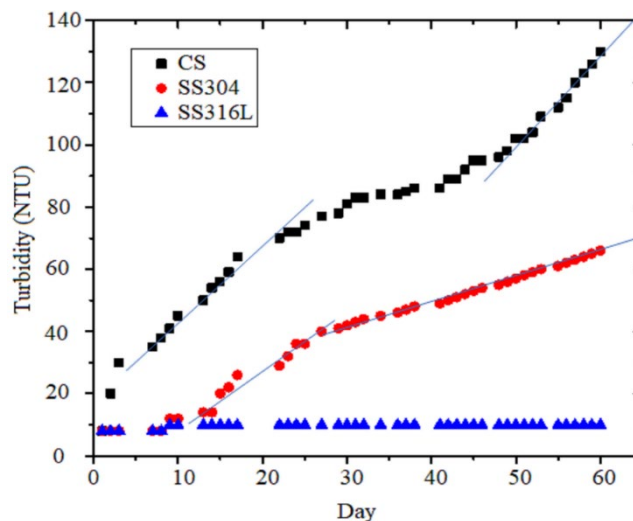


Figure 4. Turbidity of  $\text{H}_2\text{SO}_4$  solution changes as the specimens were immersed.

from day 10 to day 25 and the second slope runs from day 25 to day 60. When immersed with the SS304 specimen, the solution's turbidity is less than it is with the CS specimen. The CS and SS304 behave similarly, despite this. Up to the end of the 120-day testing period, there had been very little change in the turbidity of the solution when the SS316L specimen was immersed in it.

Turbidity changes in the  $\text{H}_2\text{SO}_4$  solution can be separated into two-time ranges: 0 day to 30 day and more than 30 days. Iron sulfate ( $\text{FeSO}_4$ ), iron oxide ( $\text{Fe}_2\text{O}_3$ ) and chromium oxide ( $\text{Cr}_2\text{O}_3$ ) suspensions in the solution and changes in the chemical characteristics of the solution cause an increase in turbidity. Turbidity in the solution is caused by metal corrosion and the formation of a passive layer where the metal ions and acid solution meet. As the concentrated  $\text{H}_2\text{SO}_4$  was diluted, both the solubility of the  $\text{FeSO}_4$  and the rate of corrosion of CS increased. When the acid concentration is less than 70 wt%, the solubility of the  $\text{FeSO}_4$  and the rate of CS corrosion increase and approach their maximum levels [1].

### 3.2.2 Volume change of $\text{H}_2\text{SO}_4$ solution

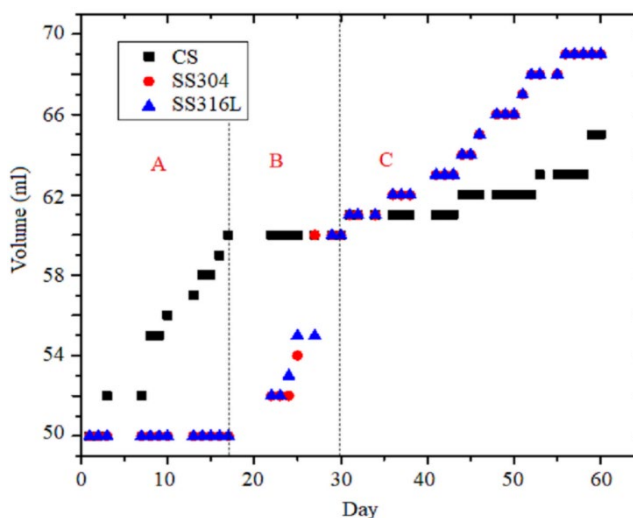


Figure 5. The volume changes of  $\text{H}_2\text{SO}_4$  solution under the different specimen immersions.

The volume of the H<sub>2</sub>SO<sub>4</sub> solution changed as the CS, SS304, and SS316L were immersed in it, as shown in Figure 5. This transformation is divided into three time periods: day 0 to day 17 (Period A), day 17 to day 30 (Period B), and day 30 and on (Period C). When Period A was considered, the solution in the bottle containing the CS specimen was significantly raised whereas the solution the SS304 and SS316L specimens remained unchanged. During Period B, the solution volume of CS specimen remained relatively constant, whereas the solution volume of SS304 and SS316L specimens increased significantly at roughly the same rate. Finally, after day 30 of the experiment, when immersed in those three specimens, the solution volume increased.

The humidity in the laboratory is controlled to 50 ± 20% RH. This moist air is continuously exposed to 98 wt% concentration of acid solution. The moist atmosphere is easily absorbed by the concentrated H<sub>2</sub>SO<sub>4</sub> surface than the diluted acid. As a result, concentrated acid levels dropped, and corrosion increased. CS has the lowest corrosion resistance and SS316L has the highest. When corrosion occurs, more moisture can be absorbed, causing the solution volume to increase.

### 3.2.3 Concentration and density of H<sub>2</sub>SO<sub>4</sub> solution

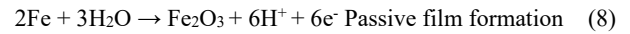
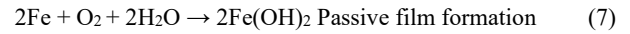
Table 2 shows the variation of concentration (%) and density (g·cm<sup>-3</sup>) of H<sub>2</sub>SO<sub>4</sub> acid when immersed with CS, SS304 and SS316L specimens for 0 days, 30 days, and 60 days. The density of H<sub>2</sub>SO<sub>4</sub> decreased for 0.2205 g·cm<sup>-3</sup>, 0.2114 g·cm<sup>-3</sup>, and 0.1604 g·cm<sup>-3</sup> after 30 days and 0.3591 g·cm<sup>-3</sup>, 0.3397 g·cm<sup>-3</sup>, and 0.3281 g·cm<sup>-3</sup> after 60 days, respectively. Immersion with CS and SS304 caused a significant drop in the density of H<sub>2</sub>SO<sub>4</sub>. Days 0 to 30 of the experiment had a decrease that is twice as great as days 30 to 60. The density of H<sub>2</sub>SO<sub>4</sub> steadily decreased in SS316L specimen from 1-60 days. This results from the effects of moisture and solution corrosion, as one might predict. The association between density and H<sub>2</sub>SO<sub>4</sub> solution concentration displayed a consistent scientific trend.

The results show that the humid environment was absorbed into concentrated H<sub>2</sub>SO<sub>4</sub>. It turns into an acid dilution with a reduced density and concentration. Corrosive acceleration occurs when acid is diluted to less than 90 weight percent. A modest amount of H<sub>2</sub>SO<sub>4</sub> solution left at room temperature frequently causes corrosion on the surface of CS. Tanks, pipes, and nozzle surfaces wetted by H<sub>2</sub>SO<sub>4</sub> should have a corrosion allowance of between 3.2 mm and 6.4 mm, depending on the acid concentration (88 wt% to 99.5 wt%) [19].

### 3.3 Corrosion mechanism

CS (3a), SS304 (3b), and SS316L (3c) specimens with concentrated H<sub>2</sub>SO<sub>4</sub> acid exposed to their surfaces are shown schematically in

Figure 6. The reactions of H<sub>2</sub>SO<sub>4</sub> acid exposed on a CS surface can be summarized as follows [20]:



According to reaction Equation (3-8), the end results of the corrosion process are typically ferrous sulfate (FeSO<sub>4</sub>), ferrous hydroxide (Fe(OH)<sub>2</sub>), ferrous oxide (Fe<sub>2</sub>O<sub>3</sub>), and hydrogen gas (H<sub>2</sub>). FeSO<sub>4</sub> is a thin, white film layer that adheres to the surface of CS only moderately well. As a result, it might be disrupted by the acid or H<sub>2</sub> gas diffusion velocities. This disruption quickly speeds up corrosion until the FeSO<sub>4</sub> film reforms again [1]. The hydroxo complex ion that results from proton transfer to solution gives the pure Fe(OH)<sub>2</sub> its white color, whereas the Fe<sub>2</sub>O<sub>3</sub> is light yellow or reddish rust. Regarding the H<sub>2</sub> component and H<sub>2</sub>O will also be a byproduct. The

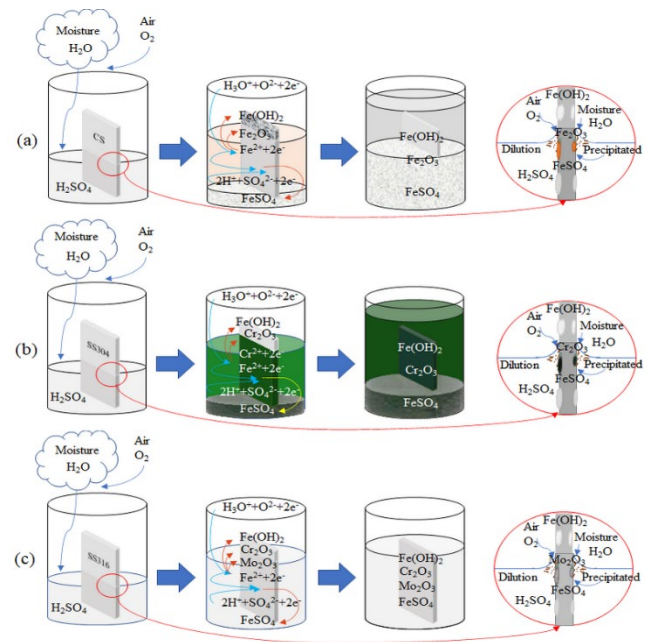
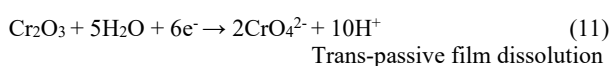


**Figure 6.** The corrosion mechanism and degradation of H<sub>2</sub>SO<sub>4</sub> acid with (a) CS, (b) SS304 (b), and (c) SS316L specimens.

**Table 2.** The concentration (%) and density (g·cm<sup>-3</sup>) of H<sub>2</sub>SO<sub>4</sub> acid when immersed with CS, SS304 and SS316L specimens for 0 day, 30 day, and 60 days.

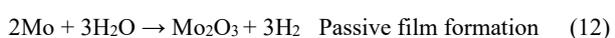
Materials	Properties	0 Days	30 Days	60 Days
CS	Concentrations (%)	98.47	70.51	58.06
	Density (g·cm <sup>-3</sup> )	1.8407	1.6202	1.4816
SS304	Concentrations (%)	98.55	70.95	60.15
	Density (g·cm <sup>-3</sup> )	1.8407	1.6293	1.5010
SS316L	Concentrations (%)	98.64	75.53	60.95
	Density (g·cm <sup>-3</sup> )	1.8407	1.6803	1.5126

H<sub>2</sub>O is one of the factors contributing to the increase in H<sub>2</sub>SO<sub>4</sub> acid levels and decrease in concentration in the storage tank. At the same time, the H<sub>2</sub> gas diffuses into the FeSO<sub>4</sub> film as it quickly rises to the surface. Eventually, it penetrates deeply into the metal's groves and can collect in the shell plates or any other cavities, where the remaining metal that is too weak can eventually split off. Corrosion is influenced by solubility, temperature, and relative movement [21]. Moreover, the use of anode protection is very efficient in this case because the FeSO<sub>4</sub> layer is formed into a crystalline film layer of Fe<sub>2</sub>O<sub>3</sub> mixed with Fe<sub>2</sub>(SO<sub>4</sub>)<sub>3</sub>·5H<sub>2</sub>SO<sub>4</sub> and FeSO<sub>4</sub>·3H<sub>2</sub>SO<sub>4</sub>, which has higher corrosion resistance than a single layer [22]. When concentrated H<sub>2</sub>SO<sub>4</sub> acid is exposed to SS304 specimen surface as seen in Figure 6(b), the reactions are represented by Equation (9-11) [19]:



When SS304 was submerged in concentrated H<sub>2</sub>SO<sub>4</sub> acid. H<sub>2</sub>SO<sub>4</sub> reacts with SS304, and then makes iron (II) sulfate which is pale green color. However, iron (II) is not stable, it is transformed into iron (III) oxide is a red-brown color or iron (III) sulfate is a cloud white color in precipitation. The strong reducing agent Cr<sup>2+</sup> rapidly reacts with H<sub>2</sub>SO<sub>4</sub> to produce chromium oxide (Cr<sub>2</sub>O<sub>3</sub>), which disperses and dissolves in the acid [23]. After 30 days and 60 days of the experiment, these ion complexes transformed the H<sub>2</sub>SO<sub>4</sub> from a clear solution into a green solution. On the metal surface, a thin Cr<sub>2</sub>O<sub>3</sub> layer in the colors glossy white and matte black was seen to have many pores. The divalent chromium ion is dispersed on the metal surface at the anode in the active state, while Cr<sub>2</sub>O<sub>3</sub> is formed in the passive state. whenever the metal surface of the anode exhibits a chromic oxide coating. This is followed by the trans-passive decomposition of the chromium oxidizer, which dissolves to produce trivalent comic oxide in the form of hexavalent chromate ions in acid solution. Furthermore, it was discovered that chromate ions cause the passive coating of chromic-ferric mixed oxides to form on metal surfaces because of iron in the metal being oxidized (CrO<sub>4</sub><sup>2-</sup>). The surface metal can be passivated using the strongest oxidizing chromate. The pH reduction and the rise in the corrosion area of the surrounds have been impacted by some aspects of the migration and diffusion of precipitate metal ion hydroxides or oxides. Moreover, the SO<sub>4</sub><sup>2-</sup> ion in the solution is likely to penetrate the passive film and damage its compactness. [23].

A schematic drawing of the SS316L specimen exposed in the concentrated H<sub>2</sub>SO<sub>4</sub> acid solution is shown in Figure 3(c). The reactions that occurred can be represented by Equations (3-11) and Equation (12), respectively [3]:



The acid solution of the SS316L specimen has no precipitation and is clear throughout the experiment. In dynamic equilibrium, the passive film interface on the SS316L is formed and decomposed competitively all the time. Cr ions (as a stronger oxidant) can better

bind oxygen atoms and convert them to Cr oxides and hydroxides, promoting passive film repairing [24]. Several studies have found that the high density of the oxide film on the surface, as well as the structural, composition, and thickness of the passive film on the surface, influence the corrosion resistance of stainless steel in H<sub>2</sub>SO<sub>4</sub> acid [25].

#### 4. Conclusions

In conclusion, the corrosion resistance of the SS316L in concentrated H<sub>2</sub>SO<sub>4</sub> acid is higher than that of the CS and SS304. Thus, SS316L is safer, and the service life is longer for the process industry materials. The corrosion mechanism depended on the formation of passive oxide film on material surfaces including Fe<sub>2</sub>O<sub>3</sub>, Cr<sub>2</sub>O<sub>3</sub> and Mo<sub>2</sub>O<sub>3</sub>. The degradation of concentrated H<sub>2</sub>SO<sub>4</sub> depends on the CS, SS304, and SS316L specimens immersion and humidity in environment. The H<sub>2</sub>SO<sub>4</sub> volume increased while its concentration and density decreased because of the moisture absorption. Moreover, the H<sub>2</sub>SO<sub>4</sub> solution has changed color and turbidity. The results indicate the selection of suitable materials for a specific industrial application constrained by the characteristics of the environment and the expected lifecycle expenses.

#### Acknowledgements

The authors would like to thank Mr. Somchai valuedrtpoonphol and teamwork at Witcorp Products Ltd. for their support and value advice on this research work. Financial support from Witcorp Products Ltd. is appreciated.

#### References

- [1] Z. Panossian, N. L. Almeida, R. M. R. de Sousa, G. de S. Pimenta, and L. B. S. Marques, "Corrosion of carbon steel pipes and tanks by concentrated sulfuric acid: A review," *Corrosion Science*, vol. 74, pp. 1-11, 2012.
- [2] T. Massoud, V. Maurice, L. H. Klein, and P. Marcus, "Nanoscale morphology and atomic structure of passive films on stainless steel," *Journal of The Electrochemical Society*, vol. 160, pp. C232-C238, 2013.
- [3] V. S. Saji, and C.-W. Lee, "Molybdenum, Molybdenum oxides, and their electrochemistry," *ChemSusChem*, vol. 5, pp. 1146-1161, 2012.
- [4] P. Marcus, V. Maurice, and H.-H. Strehblow, "Localized corrosion (pitting): A model of passivity breakdown including the role of the oxide layer nanostructure," *Corrosion Science*, vol. 50, pp. 2698-2704, 2008.
- [5] B. Zhang, Y. Li, and F. Wang, "Electrochemical corrosion behaviour of microcrystalline aluminium in acidic solutions," *Corrosion Science*, vol. 49, no. 5, pp. 2071-2082, 2007.
- [6] S. V. Muley, A. N. Vidvans, G. P. Chaudhari, and S. Udainiya, "An assessment of ultra-fine grained 316L stainless steel for implant applications," *Acta Biomaterialia*, vol. 30, pp. 408-419, 2016.
- [7] M. Tingjiang, and X. Naixin, "The galvanostatic potential oscillations of mild steel in 93% sulfuric acid," *Corrosion Science*, vol. 34, pp. 915-920, 1993.

- [8] W. Kuang, X. Wu, and E.-H. Han, "The oxidation behaviour of 304 stainless steel in oxygenated high temperature water," *Corrosion Science*, vol. 52, pp. 4081-4087, 2010.
- [9] P. Keller, and H.-H. Strehblow, "XPS investigations of electrochemically formed passive layers on Fe/Cr alloys in 0.5 M H<sub>2</sub>SO<sub>4</sub>," *Corrosion Science*, vol. 46, pp. 1939-1952, 2004.
- [10] M. Lodhi, K. Deen, and W. Haider, "Corrosion behavior of additively manufactured 316L stainless steel in acidic media," *Materialia*, vol. 2, pp. 111-121, 2018.
- [11] L. Monaco, G. Avramovic-Cingara, G. Palumbo and U. Erb, "Corrosion behaviour of electrodeposited nanocrystalline nickel-iron (NiFe) alloys in dilute H<sub>2</sub>SO<sub>4</sub>," *Corrosion Science*, vol. 130, pp. 103-112, 2018.
- [12] A. Pardo, M. C. Merino, M. Carboneras, F. Viejo, R. Arrabal, and J. Munoz, "Influence of Cu and Sn content in the corrosion of AISI 304 and 316 stainless steels in H<sub>2</sub>SO<sub>4</sub>," *Corrosion Science*, vol. 8, pp. 1075-1092, 2006.
- [13] J. Ding, Z. Lei, L. Minxu, W. Jing, W. Zhibin, and H. Wenhui, "The electrochemical behaviour of 316L austenitic stainless steel in Cl<sup>-</sup> containing environment under different H<sub>2</sub>S partial pressures," *Applied Surface Science*, vol. 289, pp. 33-41, 2014.
- [14] Q. Guo, J. Liu, M. Yu, and S. Li, "Effect of passive film on mechanical properties of martensitic stainless steel 15-5 pH in a neutral NaCl solution," *Applied Surface Science*, vol. 327, pp. 313-320, 2015.
- [15] R. Sueptitz, K. Tschulik, M. Uhlemann, L. Schultz, and A. Gebert, "Effect of high gradient magnetic fields on the anodic behaviour and localized corrosion of iron in sulphuric acid solutions," *Corrosion Science*, vol. 53, pp. 3222-3230, 2011.
- [16] R. T. Loto, C. A. Loto, A. P. I. Popoola, and M. Ranyaoa, "Corrosion resistance of austenitic stainless steel in sulphuric acid," *International journal of physical sciences*, vol. 7, pp. 1677-1688, 2012.
- [17] H. Luo, C. Dong, K. Xiao, and X. Li, "The passive behaviour of ferritic stainless steel containing alloyed tin in acidic media," *The Royal Society of Chemistry*, vol. 6, pp. 9940-9949, 2016.
- [18] Z. Wang, L. Zhang, X. Tang, Z. Zhang, and M. Lu, "The surface characterization and passive behavior of Type 316L stainless steel in H<sub>2</sub>S-containing conditions," *Applied Surface Science*, vol. 423, pp. 457-464, 2017.
- [19] NACE, *RP0391-2001: Standard Recommended Practice – Materials for the Handling and Storage of Commercial Concentrated (90 to 100%) Sulfuric Acid at Ambient Temperatures* Houston: National Association of Corrosion Engineers. 2001.
- [20] Y. Li, M. Ives, K. Coley, and J. Rodda, "Corrosion of nickel-containing stainless steel in concentrated sulphuric acid," *Corrosion Science*, vol. 46, pp. 1969-1979, 2004.
- [21] B. T. Ellison, and W. R. Schmeel, "Corrosion of steel in concentrated sulfuric acid," *Journal of The Electrochemical Society*, vol. 125, pp. 524-531, 1978.
- [22] J. Hines, and R. Williamson, "Anodic behaviour of mild steel in strong sulphuric acid-I. Steady-state conditions," *Corrosion Science*, vol. 4, pp. 201-210, 1964.
- [23] S. Jeon, H. Kim, K. Kong, and Y. Park, "Effects of copper addition on the passivity and corrosion behavior of 27Cr-7Ni hyper duplex stainless steels in sulfuric acid solution," *Materials transactions*, vol. 56, pp. 78-84, 2015.
- [24] J. Wang, J. Wang, and E.-H. Han, "Influence of conductivity on corrosion behavior of 304 stainless steel in high temperature aqueous environment," *Journal of Materials Science & Technology*, vol.32, pp. 333-340, 2016.
- [25] H. Sun, X. Wu, and E.-H. Han, "Effects of temperature on the oxide film properties of 304 stainless steel in high temperature lithium borate buffer solution," *Corrosion Science*, vol. 51, pp. 2840-2847, 2009.